Journal of Geodesy (2003) 77: 279–291
DOI 10.1007/s00190-003-0325-6

Journal of Geodesy

Orthometric corrections from leveling, gravity, density and elevation data: a case study in Taiwan

C. Hwang, Y.-S. Hsiao

Department of Civil Engineering, National Chiao Tung University, 1001 Ta Hsueh Road, Hsinchu 300, Taiwan
e-mail: hwang@geodesy.cv.nctu.edu.tw; Tel.: +886-3-5724739; Fax: +886-3-5716257

Received: 5 August 2002 / Accepted: 21 February 2003

Abstract. A new orthometric correction (OC) formula is presented and tested with various mean gravity reduction methods using leveling, gravity, elevation, and density data. For mean gravity computations, the Helmert method, a modified Helmert method with variable density and gravity anomaly gradient, and a modified Mader method were used. An improved method of terrain correction computation based on Gaussian quadrature is used in the modified Mader method. These methods produce different results and yield OCs that are greater than 10 cm between adjacent benchmarks (separated by ~2 km) at elevations over 3000 m. Applying OC reduces misclosures at closed leveling circuits and improves the results of leveling network adjustments. Variable density yields variation of OC at millimeter level everywhere, while gravity anomaly gradient introduces variation of OC of greater than 10 cm at higher elevations, suggesting that these quantities must be considered in OC. The modified Mader method is recommended for computing OC.

Keywords: Gravity anomaly gradient – Geoid – Orthometric correction – Mean gravity – Terrain correction

1 Introduction

The orthometric height (OH) can be obtained by spirit leveling (see e.g. Heiskanen and Moritz 1967; Moffit and Bossler 1998). However, height differences from leveling must be corrected for non-parallel equipotential surfaces using the orthometric correction (OC) in order to obtain OHs (Heiskanen and Moritz 1967, Chap. 4). Recent work on the OC can be found in, for example, Strang van Hees (1992), Kao et al. (2000) and Allister and Featherstone (2001). Dennis and Featherstone (2003) discuss various height systems and their advantages and disadvantages in practical applications. Rigorous OC computation is expensive because it requires observed gravity values at benchmarks along the leveling route. Also, the conventional thought is that the OC is small, especially in areas of low elevation, so it can be neglected in most cases. As already mentioned in Heiskanen and Moritz (1967), different methods for the OC may yield different OHs and the differences can reach several centimeters. This implies that OHs from leveling may mismatch the true orthometric heights by several centimeters if the OC computation is not sufficiently accurate.

It is common practice to evaluate the precision of a gravimetric geoid model by comparing modeled geoidal height with 'geoidal' heights computed from the difference between GPS-determined ellipsoidal heights and the 'orthometric heights' obtained from leveling. As just stated, OHs from leveling could be in error by several centimeters if the OC is not applied or is not properly applied. Recent progress in both theory and numerical technique has greatly improved the precision of geoid modeling, and a sub-centimeter accuracy appears within reach (see e.g. Sansò and Rummel 1997). Thus, incorrect OHs from leveling will make such geoid model evaluation unreliable. Furthermore, use of incorrect OHs for geoid model evaluation will be very likely to occur over a region with a rugged terrain and high mountains, for example the Rocky Mountains in North America, the Alps in Europe, and the Central Range in Taiwan (see below). In view of the popular use of GPS and geoid modeling for OH determination today, the subject of OC deserves more attention.

One approximation of the OH is used in Taiwan, and in earlier vertical networks normal gravity was used to convert leveling heights to OHs. In a recent effort by the Ministry of the Interior of Taiwan to completely revise Taiwan's vertical datum, leveling and gravity data have been collected at Taiwan's first-order benchmarks. Elevation, density, and gravity data are also available from other sources, for example the Institute of Agricultural and Forestry Aerial Survey, and the Institute of Earth Sciences, Academia Sinica (Yen et al. 1990). In this

Correspondence to: C. Hwang

paper, these data will be used to investigate the theories and methods of OC, for which Taiwan is an ideal testing area because of its rugged terrain and complex geological structure. In the following sections, a new OC formula will be derived and results of OC computations using various gravity reduction methods over Taiwan will be presented.

2 Theories

2.1 Orthometric height and orthometric correction

The OH is the height above the geoid measured along the curved plumb line. Leveling alone will yield a geometric height difference between two consecutive benchmarks, which in turn yields an OH difference by applying the OC (Heiskanen and Moritz 1967, Chap. 4). Thus the OC plays a critical role in obtaining OHs from leveling. A new OC formula is derived below. By definition, the OH (H) at a benchmark is the ratio between its geopotential number (C) and its mean gravity along the plumb line ($\bar{g}$) between the surface and the geoid. Thus, for two benchmarks A and B

$$\begin{aligned} H_A &= \frac{C_A}{\bar{g}_A} \\ H_B &= \frac{C_B}{\bar{g}_B} \end{aligned} \tag{1}$$

The difference between H_A and H_B is

$$\begin{aligned} \Delta H_{AB} &= H_B - H_A \\ &= \frac{C_B}{\bar{g}_B} - \frac{C_A}{\bar{g}_A} \\ &= \frac{1}{\bar{g}_B}(C_B - C_A) + \frac{C_A}{\bar{g}_B} - \frac{C_A}{\bar{g}_A} \\ &= \frac{1}{\bar{g}_B}\int_A^B g \, \mathrm{d}n + \frac{C_A}{\bar{g}_B} - \frac{C_A}{\bar{g}_A} \end{aligned} \tag{2}$$

where $\mathrm{d}n$ is the differential geometric increment of height and $g\,\mathrm{d}n = \mathrm{d}C$, with g being surface gravity. Furthermore

$$\frac{C_A}{\bar{g}_B} - \frac{C_A}{\bar{g}_A} = H_A\left(\frac{\bar{g}_A}{\bar{g}_B} - 1\right) \tag{3}$$

and

$$\begin{aligned} \frac{1}{\bar{g}_B}\int_A^B g \, \mathrm{d}n &= \frac{1}{\bar{g}_B}\int_A^B (g - \bar{g}_B + \bar{g}_B)\mathrm{d}n \\ &= \int_A^B \mathrm{d}n + \frac{1}{\bar{g}_B}\int_A^B (g - \bar{g}_B)\mathrm{d}n \\ &\approx \sum_{i=1}^{k} \delta n_i + \frac{1}{\bar{g}_B}\sum_{i=1}^{k}(g_i - \bar{g}_B)\delta n_i \\ &= \Delta n_{AB} + \frac{1}{\bar{g}_B}\sum_{i=1}^{k}(g_i - \bar{g}_B)\delta n_i \end{aligned} \tag{4}$$

where Δn_{AB} is the sum of all geometric height differences between A and B obtained directly from leveling, g_i is surface gravity value at leveling set i, δn_i is the geometric height difference at leveling set i, and k is the number of sets. A leveling set may span up to 100 m horizontal distance between backsight and foresight, depending on the terrain and the level used (see e.g. Moffit and Bossler 1998). In Eq. (4), the two integrals have been approximated by finite, discrete sums. Substituting Eqs. (3) and (4) into Eq. (2) yields

$$\Delta H_{AB} = \Delta n_{AB} + \frac{1}{\bar{g}_B}\sum_{i=1}^{k}(g_i - \bar{g}_B)\delta n_i + H_A\left(\frac{\bar{g}_A}{\bar{g}_B} - 1\right) \tag{5}$$

Thus an OC formula is obtained as

$$OC_{AB} = \frac{1}{\bar{g}_B}\sum_{i=1}^{k}(g_i - \bar{g}_B)\delta n_i + H_A\left(\frac{\bar{g}_A}{\bar{g}_B} - 1\right). \tag{6}$$

This formula is to be compared with the formula given by Heiskanen and Moritz (1967, p. 168)

$$OC_{AB}^{HM} = \sum_{i=1}^{k}\frac{g_i - \gamma_0}{\gamma_0}\delta n_i + \frac{\bar{g}_A - \gamma_0}{\gamma_0}H_A - \frac{\bar{g}_B - \gamma_0}{\gamma_0}H_B \tag{7}$$

where γ_0 is normal gravity at some latitude (usually 45°N or 45°S). If A is sufficiently close to B in horizontal distance (below 2 km), Eq. (6) can be simplified as follows. Within a short distance, gravity can be assumed to be a linear function of height, as well as horizontal distance. Then, Eq. (4) gives

$$\frac{1}{\bar{g}_B}\int_B^A (g - \bar{g}_B)\mathrm{d}n = \frac{1}{\bar{g}_B}\left(\frac{g_A + g_B}{2} - \bar{g}_B\right)\Delta n_{AB} \tag{8}$$

Thus, a simplified formula for the OC is

$$OC_{AB} = \frac{1}{\bar{g}_B}\left(\frac{g_A + g_B}{2} - \bar{g}_B\right)\Delta n_{AB} + H_A\left(\frac{\bar{g}_A}{\bar{g}_B} - 1\right) \tag{9}$$

where g_A and g_B are the surface gravity values at A and B. From Eq. (9) and the assumptions used to derive it, gravity values need only be measured at the two adjacent benchmarks (A and B in this case), without knowing the gravity values at the k leveling sets between them. As an example, Fig. 1 shows the relationship between gravity and elevation collected at 32 leveling sets along a 2-km-long leveling line in central Taiwan. The mean elevation here is approximately 1800 m and the height difference between the start and end benchmarks is approximately 100 m. In this case, the gravity values are almost linearly correlated with elevation. For this particular leveling line, the OC was computed using Eq. (9) and the more rigorous Eq. (6). The difference in OC is less than 0.1 mm. Thus, the small perturbation from linearity should have little effect on the accuracy of the approximation in Eq. (9).

In Eq. (9) it remains to determine the mean gravity values along the plumb lines at A and B. A simple

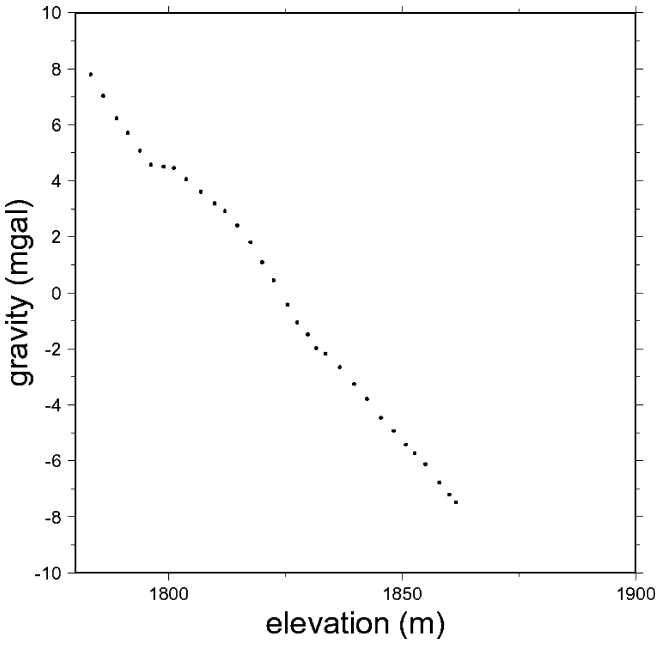

Fig. 1. Relationship between elevation and gravity along a 2-km-long leveling line at approximately longitude 121°9′34″ and latitude 24°2′59″. A mean value of 978 469.308 mGal is removed from the gravity values

method of mean gravity computation is based on the Poincaré–Prey reduction, where the topographic effect of only the Bouguer plate is considered. This assumes that the vertical gravity gradient and density are constant along the plumb line. By setting Q on the geoid in Eq. (4–2) of Heiskanen and Moritz (1967, p. 164) and then taking the average value of the surface gravity and the gravity on the geoid, the mean gravity along the plumb line can be computed by (cf. Heiskanen and Moritz 1967, p. 167)

$$\bar{g} = g - \left(\frac{1}{2}\frac{\partial g}{\partial h} + 2\pi K\rho\right)H \tag{10}$$

where g is surface gravity, $\partial g/\partial h$ is free-air gravity gradient, ρ is rock density, K is the gravitational constant, and H is height (here H is the approximate OH from leveling without applying the OC). The free-air gravity gradient can be split into the normal gravity gradient and gravity anomaly gradient

$$\frac{\partial g}{\partial h} = \frac{\partial \gamma}{\partial h} + \frac{\partial \Delta g}{\partial H} \tag{11}$$

where γ and Δg are normal gravity and the gravity anomaly, respectively. The linear normal gradient is approximately -0.3086 mGal m^{-1}. If the gravity anomaly gradient is neglected and the rock density is assumed to be 2.67 g cm^{-3}, then an approximate formula for computing mean gravity along the plumb line is

$$\bar{g} = g + 0.0424H. \tag{12}$$

The use of mean gravity computed by Eq. (12) in Eq. (1) yields the Helmert OH.

2.2 Error due to density variation and gravity anomaly gradient

As will be shown below, the gravity anomaly gradient over Taiwan can be very large in mountainous areas, so it cannot be neglected. Vaníček et al. (2000) reported that use of the gravity anomaly gradient will change OHs by up to a few decimeters over the Canadian Rocky Mountains. Also, rock density over Taiwan is variable and cannot be assumed to be constant. Therefore, in this paper, it will be investigated how density variations and gravity anomaly gradients affect the result of OC. From Eq. (10), variation of rock density ($\delta\rho$) gives rise to variation of mean gravity along the plumb line ($\delta\bar{g}$) as

$$\delta\bar{g} = -2\pi KH\delta\rho \tag{13}$$

which, based on Eq. (9), in turn introduces a variation in the OC as

$$\begin{aligned}\delta OC^{d}_{AB} &= \frac{\partial OC_{AB}}{\partial \bar{g}_A}\delta\bar{g}_A + \frac{\partial OC_{AB}}{\partial \bar{g}_B}\delta\bar{g}_B \\ &= \frac{2\pi K}{\bar{g}_B^2}\left[\frac{g_A + g_B}{2}(H_B - H_A)H_B\delta\rho_B \right. \\ &\quad \left. + \bar{g}_A H_A H_B \delta\rho_B - \bar{g}_B H_A^2 \delta\rho_A\right]\end{aligned} \tag{14}$$

Furthermore, the gravity anomaly gradient introduces a variation of mean gravity along the plumb line as

$$\delta\bar{g} = -1/2\Delta g_H H \tag{15}$$

where $\Delta g_H = \partial\Delta g/\partial H$. Using a similar derivation to Eq. (14), the variation in the OC due to the gravity anomaly gradient is

$$\begin{aligned}\delta OC^{g}_{AB} &= \frac{1}{2\bar{g}_B^2}\left[\frac{g_A + g_B}{2}(H_B - H_A)H_B\Delta g_{h_B} \right. \\ &\quad \left. + \bar{g}_A H_A H_B \Delta g_{h_B} - \bar{g}_B H_A^2 \Delta g_{h_A}\right]\end{aligned} \tag{16}$$

Since in our first-order leveling network any two adjacent benchmarks are only about 2 km apart, the approximations $\Delta g_{h_A} \approx \Delta g_{h_B}$ and $\bar{g}_A \approx \bar{g}_B$ may be employed in Eq. (16). Then

$$\delta OC^{g}_{AB} = \frac{\Delta g_{h_B}}{2\bar{g}_B^2}\left(\frac{g_A + g_B}{2}H_B + \bar{g}_B H_A\right)(H_B - H_A) \tag{17}$$

The gravity anomaly gradient at point p can be computed by (Heiskanen and Moritz 1967)

$$\frac{\partial\Delta g}{\partial h} = \frac{R^2}{2\pi}\iint_{\sigma}\frac{\Delta g - \Delta g_P}{l_0^3}\,\mathrm{d}\sigma - \frac{2}{R}\Delta g_P \tag{18}$$

where R is the Earth's mean radius (≈ 6371 km), Δg_P is the gravity anomaly at p, Δg is the gravity anomaly on

the unit sphere, σ is the unit sphere, $d\sigma$ is the differential element of area ($= \cos\phi\, d\phi\, d\lambda$, with ϕ and λ being latitude and longitude) and $l_0 = 2R\sin(\psi/2)$, with ψ being the spherical distance. The kernel function l_0 in Eq. (18) becomes singular when $\psi = 0$, thus the integration part in Eq. (18) can be split into two parts to avoid this singularity, i.e. symbolically

$$\frac{\partial \Delta g}{\partial h} = \frac{R^2}{2\pi}\int_0^{\sigma_0} \frac{\Delta g - \Delta g_P}{l_0^3}\, d\sigma + \frac{R^2}{2\pi}\int_{\sigma_0}^{\sigma} \frac{\Delta g - \Delta g_P}{l_0^3}\, d\sigma - \frac{2}{R}\Delta g_P = A + B + C \tag{19}$$

where σ_0 is the innermost zone (see later discussion). It turns out that the C term is very small compared to the A and B terms, so it can be neglected. For example, in the extreme case of $\Delta g_p = 370$ mGal at a benchmark of elevation $H_p = 3500$ m near the highest spot in the Central Range of Taiwan, the C term will contribute $CH_p/2 = 0.2$ mGal to the mean gravity [see Eqs. (10) and (11)]. The A term is the innermost-zone effect and can be computed by (Heiskanen and Moritz 1967, p. 122)

$$A = \frac{s_0}{4}(g_{xx} + g_{yy}) \tag{20}$$

where s_0 is the radius of the innermost zone, which can be approximated as $s_0 = \sqrt{(\Delta x \Delta y/\pi)}$, with Δx and Δy being the planar grid intervals in the east and north directions, and g_{xx} and g_{yy} the second derivatives of the gravity anomaly along the east and north directions. In the practical computations of the innermost-zone effect, a quadratic polynomial is least-squares (LS) fitted to the gridded gravity anomalies and then g_{xx} and g_{yy} are obtained from the second derivatives of the polynomial.

The B term in Eq. (19) can be computed by Gaussian quadrature (see e.g. Gerald and Wheatley 1994). Let the B term be expressed as

$$\begin{aligned} B &= \frac{R^2}{2\pi}\int_{\sigma_0}^{\sigma} \frac{\Delta g - \Delta g_P}{l_0^3}\, d\sigma \\ &= \frac{1}{16\pi R}\int_{\lambda}\int_{t} \frac{\Delta g - \Delta g_P}{\sin^3\frac{\psi}{2}}\, dt\, d\lambda \\ &\approx \frac{1}{16\pi R}\int_{t_{\min}}^{t_{\max}} \left[\int_{\lambda_{\min}}^{\lambda_{\max}} g(t,\lambda)\, d\lambda\right] dt \\ &= \frac{1}{16\pi R}\int_{t_{\min}}^{t_{\max}} k(t)\, dt \end{aligned} \tag{21}$$

where $\lambda_{\min}$ and $\lambda_{\max}$ are the longitudes of the western and eastern borders of the computational area, and $t_{\min} = \sin(\phi_{\min}), t_{\max} = \sin(\phi_{\max})$, with $\phi_{\min}$ and $\phi_{\max}$ being the latitudes of the southern and northern borders. Extending the one-dimensional (1-D) Gaussian quadrature formula to the two-dimensional (2-D) case yields

$$B \approx \sum_{i=1}^{M} w_i^t k(t_i) \tag{22}$$

with

$$k(t) = \int_{\lambda_{\min}}^{\lambda_{\max}} g(t,\lambda)\, d\lambda \approx \sum_{i=1}^{N} w_i^{\lambda} g(t,\lambda_i) \tag{23}$$

where w_i^{λ} and w_i^t are weighting coefficients, and t_i and λ_i are the nodal coordinates along latitude and longitude for the domains $[\lambda_{\min}, \lambda_{\max}]$ and $[t_{\min}, t_{\max}]$, and for the chosen M and N, which are the numbers of weighting coefficients and nodes. In the computations, M and N are chosen to be the numbers of grid points along latitude and longitude, respectively. This choice of M and N yields the highest possible integration precision for the given grid. Since the gravity anomalies are given on a regular grid in latitude and longitude, interpolations using six-degree polynomials were made to obtain the function values $k(t_i)$ and $g(t,\lambda_i)$ at the unevenly spaced nodes t_i and λ_i. Use of a degree higher than six does not increase the interpolation accuracy. The program GAULEG, provided in Press et al. (1989), was used for the computations of weighting coefficients and nodal coordinates. Compared to other numerical integration methods such as Simpson's method, Gaussian quadrature requires less functional evaluations and can achieve high precision, provided that the number of weighting coefficients is sufficiently large (this will also depend on the frequency content of the function to be integrated); see also Gerald and Wheatley (1994) for discussions of the accuracy of Gaussian quadrature and other numerical integration techniques.

2.3 A modified Mader method of gravity reduction

From the definition of OH in Eq. (1), it is clear that the mean gravity along the plumb line is an important quantity that should be computed with great care. According to Dennis and Featherstone (2003) and Heiskanen and Moritz (1967), the Mader method (Mader 1954) yields a more realistic mean gravity than the Poincaré–Prey reduction method because the former takes into account the terrain effect. In this paper, the Mader method is modified to consider density variations and to use rigorous terrain corrections (TCs) and gravity gradients. Letting the surface gravity value be g_p, the procedure for OC computation for the modified Mader method is as follows (see Fig. 2).

Step 1. Remove the topographic mass above the geoid

$$g_p' = g_p + tc_{\text{surface}} - 2\pi K\rho H_p \tag{24}$$

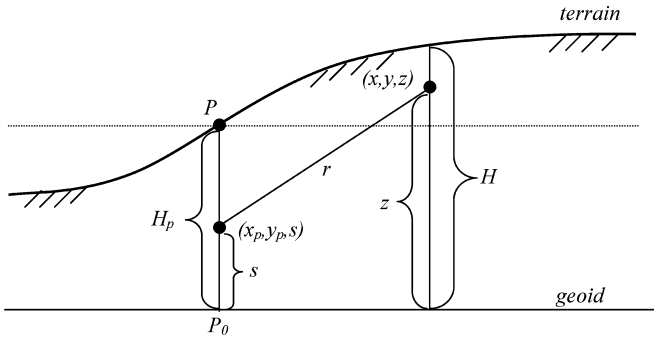

Fig. 2. Geometry for terrain corrections and reduction of mean gravity

Step 2. Apply the free-air reduction to surface gravity to approximately obtain gravity on the geoid

$$g_{p_0} = g'_p - \frac{\partial g}{\partial h} H_p \tag{25}$$

Step 3. Restore the topographic mass above the geoid

$$g'_{p_0} = g_{p_0} - 2\pi K \rho H_p - tc_{\text{sea}} \tag{26}$$

Step 4. Compute the mean gravity (as an approximation of the true mean along the plumb line)

$$\bar{g}_p = (g_p + g'_{p_0})/2 \tag{27}$$

The purpose of Step 1 is to make the 'free-air reduction' in Step 2 close to reality. Step 1 is implemented by first computing the TC to the surface gravity, tc_{surface}, and then removing the gravity effect due to the Bouguer plate. In Step 2, the vertical gravity gradient is the gradient of g'_p, which is the sum of the gradient of normal gravity and the gradient of the Bouguer anomaly (Heiskanen and Moritz 1967). The vertical gradient of the Bouguer anomaly can be computed using Eq. (19). In Step 3, the gravity effect of the mass above the geoid is the sum of the effect of the Bouguer plate and the effects of the missing mass above the level at p and the redundant mass below the level at p (the latter two effects are collected in the tc_{sea} term). In Step 4, it is again assumed that gravity is a linear function of height, so that the mean gravity is the arithmetic average of the gravity values at the surface and on the geoid.

In Steps 1 and 3, two kinds of 'terrain correction' need to be computed, one at the surface and the other at sea level. The TC at the surface, tc_{surface}, is the conventional TC seen in standard textbooks such as Heiskanen and Moritz (1967) and Torge (1989). Referring to Fig. 2, the potential at (x_p, y_p, s) due to the mass above and under the level of H_p is

$$V = K \int_x \int_y \int_{z=H_p}^{H} \frac{\rho(x,y)\, \mathrm{d}x\, \mathrm{d}y\, \mathrm{d}z}{\sqrt{(x-x_p)^2 + (y-y_p)^2 + (z-s)^2}} \tag{28}$$

Then the TC at a surface point p is

$$\begin{aligned} tc_{\text{surface}} &= \left(\frac{\partial V}{\partial s}\right)|_{s=H_p} \\ &= K \int_x \int_y \int_{z=H_p}^{H} \frac{\rho(x,y)(z-H_p)\, \mathrm{d}x\, \mathrm{d}y\, \mathrm{d}z}{[(x-x_p)^2 + (y-y_p)^2 + (z-H_p)^2]^{3/2}} \\ &= K \int_x \int_y \left[\frac{\rho(x,y)}{\sqrt{(x-x_p)^2 + (y-y_p)^2}} \right. \\ &\quad \left. - \frac{\rho(x,y)}{\sqrt{(x-x_p)^2 + (y-y_p)^2 + (H-H_p)^2}} \right] \mathrm{d}x\mathrm{d}y \\ &= K \int_x \int_y f(x,y)\mathrm{d}x\mathrm{d}y \end{aligned} \tag{29}$$

where density ρ and height H (can be OH without OC) are functions of x, y. Since $f(x, y)$ is always positive, the TC at the Earth's surface is always positive. Furthermore, the TC at the sea level point corresponding to p is

$$\begin{aligned} tc_{\text{sea}} &= \left(\frac{\partial V}{\partial s}\right)|_{s=0} = K \int_x \int_y \int_{z=H_p}^{H} \frac{\rho(x,y) z\, \mathrm{d}x\, \mathrm{d}y\, \mathrm{d}z}{[(x-x_p)^2 + (y-y_p)^2 + z^2]^{3/2}} \\ &= K \int_x \int_y \left[\frac{\rho(x,y)}{\sqrt{(x-x_p)^2 + (y-y_p)^2 + h_p^2}} \right. \\ &\quad \left. - \frac{\rho(x,y)}{\sqrt{(x-x_p)^2 + (y-y_p)^2 + H^2}} \right] \mathrm{d}x\, \mathrm{d}y \\ &= K \int_x \int_y g(x,y)\mathrm{d}x\mathrm{d}y. \end{aligned} \tag{30}$$

Depending on H_p, the function $g(x, y)$ can be positive or negative. Thus, unlike tc_{surface}, tc_{sea} can be positive or negative. For example, if on average H_p is higher than the surrounding terrain, then tc_{sea} will be negative. Linear approximations for Eq. (29), such as those given in Moritz (1968) and Schwarz et al. (1990), enable the use of fast Fourier transform (FFT) for efficient computation, but may yield a poor accuracy in the case of large terrain slope (Forsberg 1984; Schwarz et al. 1990; Tsoulis 2001). In order to achieve the highest possible precision, in this paper the Gaussian quadrature as used in Eq. (21) is used to compute the required TCs. Gaussian quadrature computes TC on a pointwise base rather than on a gridwise base as in FFT, so it will need only a little computation time if only few data points are sought. However, in the case of TC for a grid consisting of a large number of grid points, Gaussian quadrature will be slower than FFT. This is a minor problem given today's computing power.

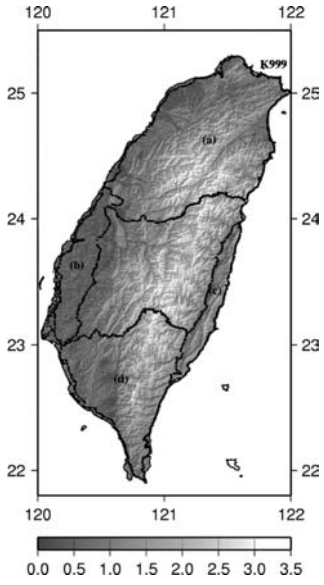

Fig. 3. A shaded-relief map of elevation over Taiwan (in km). *Solid dots* represent the 1010 first-order leveling benchmarks. (a), (b), (c), and (d) indicate four closed leveling circuits. K999 is the origin of Taiwan's vertical control network

3 Data

3.1 Leveling data

The spirit leveling data were collected in 2000 and 2001 on 1010 first-order benchmarks in a multi-year project to set up a new vertical control network for Taiwan. The total length of the leveling lines is about 2000 km. Figure 3 shows the distribution of these benchmarks, together with topography (see below). The leveling lines are situated in different terrains, ranging from plains and foothills in the western and eastern coastal areas to high mountains in the Central Range. In particular, several benchmarks are situated about 3500 m above sea level on a leveling line crossing the Central Range [the southern portion of Circuit (a) in Fig. 3]. The geometric height differences were measured by Zeiss DiNi digital levels, along with precise leveling rods graduated on ivar strips. In this measuring campaign, it was required that the difference from forward and backward leveling between two benchmarks must be less than $2.5\sqrt{K}$ mm, where K is the distance in kilometers between two adjacent benchmarks. Systematic errors due to collimation error, refraction of the atmosphere, the Earth's curvature, and a thermal effect on leveling rods have been corrected as best as possible. Approximated orthometric heights (i.e. without applying OC), which will be used in the OC computations, at these 1010 benchmarks are obtained by LS adjustment by fixing the height at Benchmark K999 to 5.6156 m at Keelung Harbor. These geometric height differences are to be corrected for OC.

3.2 Elevation data

A total of 6 421 075 point elevations were obtained from the Agricultural and Forestry Aerial Survey Institute, Taiwan, to construct regular grids for the terrain correction. The spatial resolution of these point data is about 80 m. As a first step, the coordinates of the data points were transformed to a geocentric system using the transformation parameters provided by the Ministry of the Interior, Taiwan. The GMT (Wessel and Smith 1995) routine 'surface' was then used to interpolate elevations onto regular grids with a tension factor of 0.25. A $3'' \times 3''$ grid (equivalent to a 90-m spatial resolution) and a $30'' \times 30''$ grid (equivalent to a 1-km spatial resolution) were then constructed. The first versions of elevation grids from 'surface' contained serious edge effects along the coastlines. Therefore, for the revised versions the GMT routine 'grdlandmask' was used to generate a land/ocean mask grid, which was then used to constrain the elevations at sea (i.e. to set zeros at sea). Figure. 3 shows a shaded-relief map based on the $3'' \times 3''$ elevation grid.

3.3 Gravity data

Relative gravity measurements were also collected on the 1010 first-order benchmarks shown in Fig. 3. An adjustment of these gravity measurements was carried out using the method described in Hwang et al. (2002), yielding an averaged standard deviation of 0.07 mGal for the adjusted point gravity values. These gravity values at benchmarks are the most important quantities for OC computations. In addition, three sets of point gravity data on land and one set of marine gravity data around Taiwan from Hsu et al. (1998) were also collected and compiled. The compilation involved coordinate transformation, outlier removal and use of a common normal gravity formula. Figure 4 shows the distribution of all gravity data. An empirical covariance function of the free-air gravity anomaly around Taiwan was computed. As a result of the rugged terrain and high mountains, the variance of gravity anomaly around Taiwan is 7736 mGal^2. The correlation length of the covariance function is approximately 26 km. Based on this empirical covariance function, gravity anomalies were computed on a $1' \times 1'$ grid using LS collocation (Moritz 1980). Figure 4 also shows contours of the free-air gravity anomaly. Compared to the gravity anomaly grids in Hwang (1997) and in Yen et al. (1990), the current grid has a higher spatial resolution and contains gravity features not seen before. This new gravity anomaly grid will be used to compute the gravity anomaly gradients.

3.4 Density data

The density data used in this study were provided by Chiou (1997) and are available on a $5' \times 5'$ grid. To form this density grid, Chiou (1997) first obtained the distribution of rocks over Taiwan. By associating each type of rock with an average density and using a statistical technique, Chiou (1997) then derived the $5' \times 5'$ density grid. Chiou's density model has been validated by a density model from seismology data.

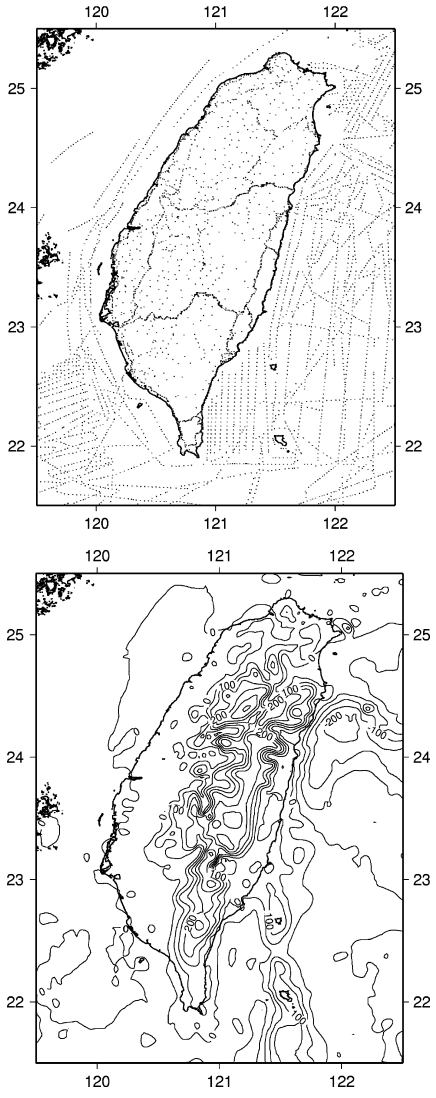

Fig. 4. Distribution of all gravity data (*top*) and contours (*bottom*) of free-air gravity anomalies from a $1' \times 1'$ grid. The contour interval is 50 mGal

Figure 5 shows a contour map of density over Taiwan. In the western coastal plains and the Longitudinal Valley in eastern Taiwan, where sediments prevail, the densities are relatively low and are mostly below 2.0 g cm^{-3}. In the foothills to the west and east of the Central Range, the densities range from 2.0 to 2.5 g cm^{-3}. In the eastern part of the Central Range, the density is highest and can reach 3.08 g cm^{-3}. The averaged density over Taiwan is 2.37 g cm^{-3}, which differs by 12% from the commonly used value of 2.67 g cm^{-3}.

4 Results

4.1 Orthometric corrections from different reductions of mean gravity

OC was computed for the geometric height differences between adjacent benchmarks for the 1010 first-order

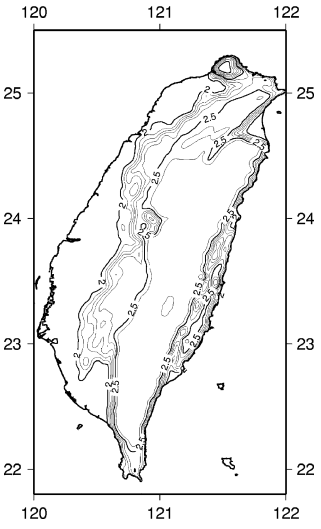

Fig. 5. Contours of rock density over Taiwan (from Chiou 1997). The contour interval is 0.1 g cm^{-3}

benchmarks (Fig. 3) using different reductions of mean gravity, all based on Eq. (9). The following five methods were used to compute mean gravity.

Method 1. Helmert method (with a constant density of 2.67 g cm^{-3}).
Method 2. Helmert method with variable density only.
Method 3. Helmert method using gravity anomaly gradient only.
Method 4. Helmert method using both variable density and gravity anomaly gradient.
Method 5. Modified Mader method.

The resulting mean gravity values are called G1, G2, G3, G4, and G5, and the corresponding OCs are called OC1, OC2, OC3, OC4, and OC5. Figure 6 shows OC1, OC4, and OC5. Figure 7 shows their differences with respect to location and height. Table 1 shows the statistics for OC. The OC was also computed using Eq. (7) (the Heiskanen and Moritz formula) with the same mean gravity as used in Method 1, and it was found that the maximum and standard deviation differences between the OC from Eq. (7) and those from Method 1 are 0.77 and 0.07 mm, respectively. Thus, the new formula in Eq. (6) produces similar results to that from Eq. (7) for a maximum height of 3500 m.

In general, for all methods, the OC is only few millimeters over plains and foothills, and is relatively large over the Central Range. In terms of standard deviation, Method 5 produces the largest OC (Table 1). Two groups of large OC occur around the terrain peaks of Circuits (a) and (d) (see Fig. 3) across the Central Range. Here the largest OC between two adjacent benchmarks is greater than 10 cm. The OCs in these two groups are nearly anti-symmetric with respect to the terrain peaks. However, it can be shown that, at high elevations, the OC is dominated by the height difference between the two adjacent benchmarks, (see also Kao et al. 2000). Since the elevation does not monotonically increase or monotonically decrease along a leveling line,

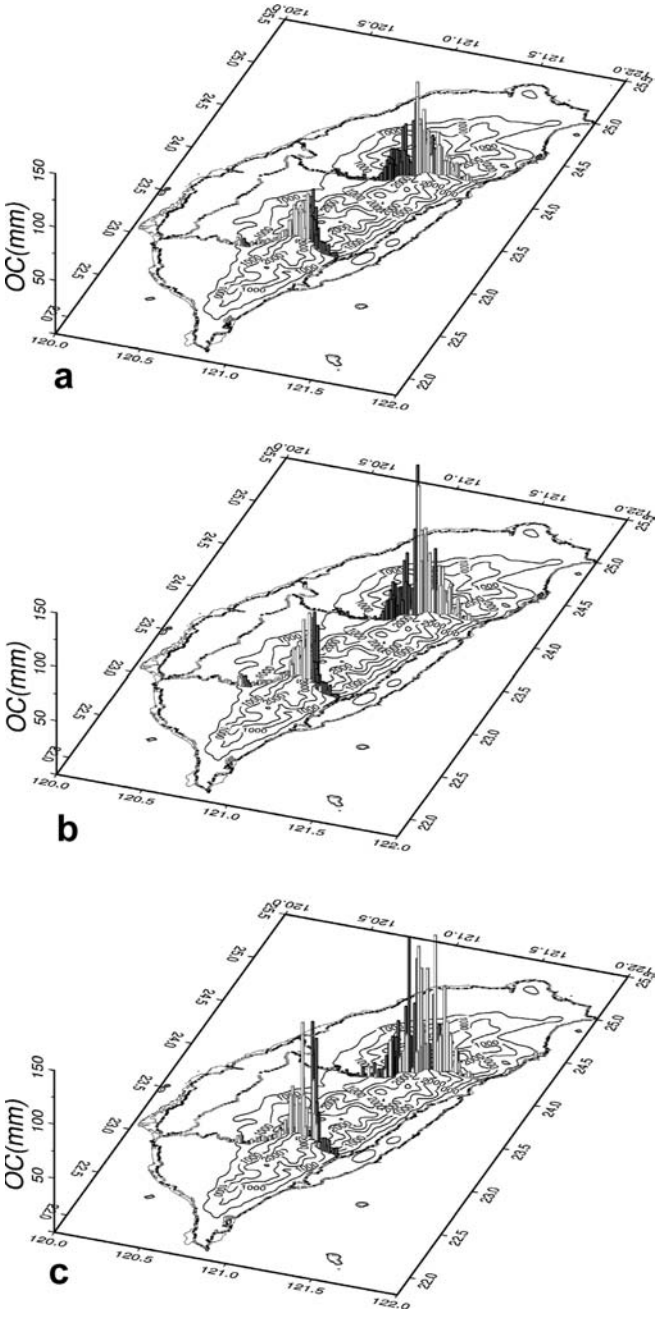

Fig. 6. Orthometric corrections from Methods **a** 1, **b** 4, and **c** 5. *Dark-gray* and *light-gray* bars indicate positive and negative OC values, respectively. *Solid lines* are contours of elevation at an interval of 500 m

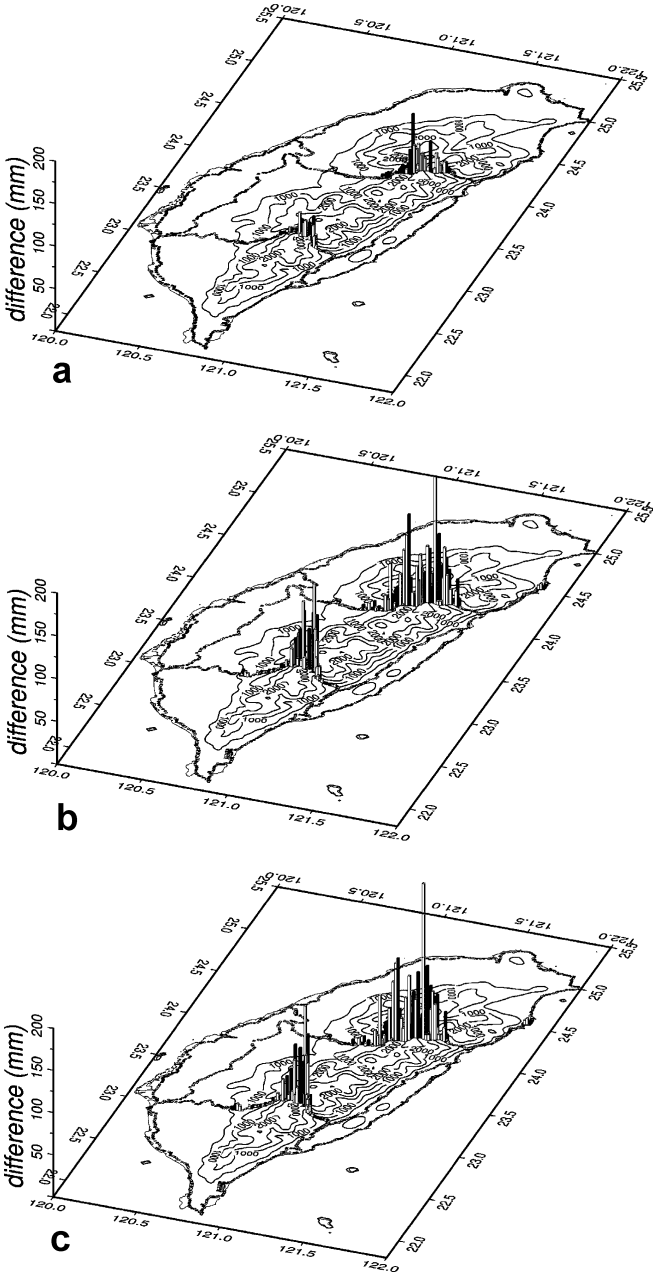

Fig. 7. Difference between **a** OC4 and OC1, **b** OC5 and OC1, and **c** OC5 and OC4. *Dark-gray* and *light-gray* bars indicate positive and negative differences, respectively. *Solid lines* are contours of elevation at an interval of 500 m

the sign of height difference may alternate in any possible manner. This alternation of the sign of height difference results in large positive and negative OCs side by side, as seen in Figs. 6 and 7.

The differences in OC from the different methods, as shown in Fig. 7, are small at low elevations and large at high elevations. The largest differences for OC4–OC1, OC5–OC1 and OC5–OC2 (see Fig. 7) are approximately 7, 14, and 18 cm, respectively. These large differences in the OCs are due to the large differences in the mean gravity used. For example, at elevation of 3 km a difference of 50 mGal in mean gravity will create a difference of 15 cm in orthometric height (Heiskanen and Moritz 1967, p. 169). Other analyses are described in the following sections.

4.2 Effects of density variation and gravity anomaly gradient on OC computation

From Table 1 it can be seen that the effect of density variation on the OC is small everywhere (maximum 3 mm at the peak of the Central Range). However,

Table 1. Statistics of orthometric corrections (in mm) between adjacent benchmarks (separated by ~ 2 km) from different methods of mean gravity reduction

Method	Maximum	Minimum	Mean	Standard deviation
Method 1 (Helmert)	69.01	−86.53	−0.04	8.68
Method 2 (Helmert with variable density)	70.79	−87.71	−0.04	8.74
Method 3 (Helmert with gravity anomaly gradient)	137.71	−118.38	−0.04	11.84
Method 4 (Helmert with variable density and gravity anomaly gradient)	139.49	−119.56	−0.04	11.93
Method 5 (modified Mader)	125.10	−124.82	−0.04	13.90

Table 2. Statistics of absolute errors in orthometric height (in mm) due to density variation and gravity anomaly gradient

Source of error	Maximum	Mean	RMS
Density variation	3.18	0.11	0.27
Gravity anomaly gradient	68.70	0.93	4.16
Density variation and gravity anomaly gradient	70.48	0.99	4.28

considering the stringent accuracy requirement of the first-order leveling and the fact that the effect is systematic, density variation cannot be neglected in the OC. In Table 1, free-air gravity anomalies are used to compute the gravity anomaly gradients. The effect of the gravity anomaly gradient on the OC is small, but significant, at low elevations, and is large at high elevations. Table 2 shows the statistics of errors in OC if density variation and gravity anomaly gradient are neglected [see Eqs. (14) and (16)]. Thus the difference between OC5 and OC1 in Fig. 7b is largely due to the gravity anomaly gradient. Figure 8 shows contours of gravity anomaly gradient and error in gravity reduction if gravity anomaly gradient is neglected (note: for the latter, half of the free-air anomaly error in Fig. 8 will be the mean gravity error). As expected, large gravity anomaly gradients exist in the Central Range, with the maximum reaching 0.02 mGal m^{-1}. Here gravity anomaly gradients introduce large errors in free-air gravity anomaly and mean gravity. As an example, at an elevation of 3 km a gravity anomaly gradient of 0.02 mGal m^{-1} will introduce an error of 30 mGal in mean gravity [see Eq. (10)], and an error of 60 mGal in the free-air gravity anomaly. The gravity anomaly gradients in plains and foothills are relatively small (typically 0.005 mGal m^{-1}). Thus, for example, at an elevation of 500 m a gravity anomaly gradient of 0.005 mGal m^{-1} will introduce an error of 1.25 mGal in mean gravity and 2.5 mGal in free-air gravity anomaly, which amounts to a sub-millimeter error in OC.

The orthometric height at a benchmark, H_p, is obtained by adding the height at the origin of the vertical control network, H_0, and the cumulative orthometric height differences between the origin and this benchmark, i.e.

$$H_p = H_0 + \sum OH_i \tag{31}$$

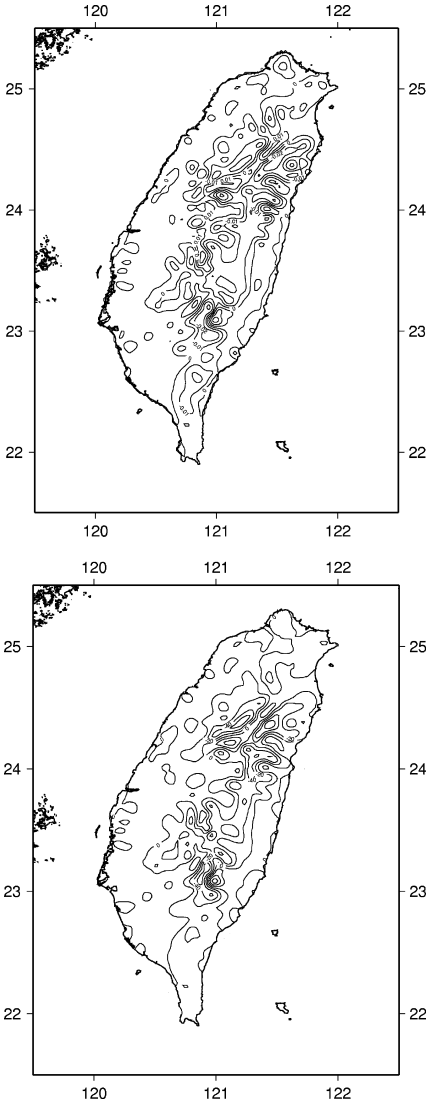

Fig. 8. Contours of the vertical gradient of free-air gravity anomaly (*top*) and the error in the free-air gravity anomaly (*bottom*) due to neglecting the gravity anomaly gradient

where OH_i is the orthometric height difference between two adjacent benchmarks. Thus the error of H_p will come entirely from the cumulative error of OH_i [Here the shift in H_0 due to the world vertical datum definition (e.g. Rapp and Balasubramania 1992) will not be discussed]. Figure 9 shows the cumulative errors along

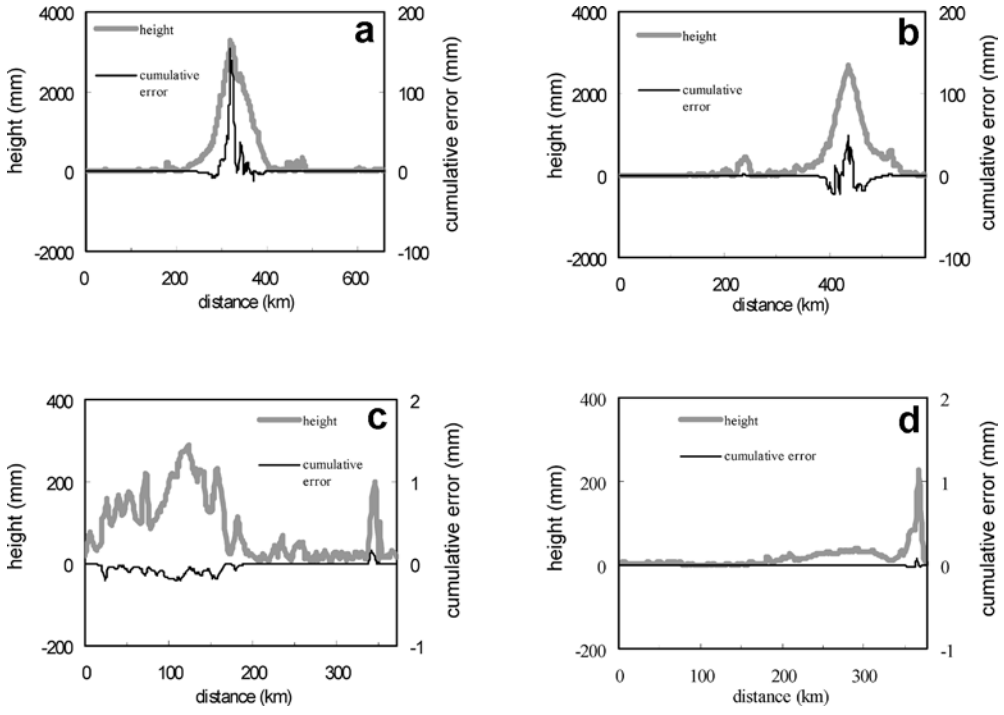

Fig. 9. Cumulative errors in orthometric height due to variable density and gravity anomaly gradient along four leveling circuits (see Fig. 3)

four closed leveling circuits (see Fig. 3). Circuit (a) has the largest cumulative OC error of 15 cm, occurring at the highest elevation of about 3500 m. This suggests that, for example, at the terrain peak of Circuit (a), the orthometric height as computed from Eq. (31) will be in error by 15 cm if density variations and gravity anomaly gradients are not taken into account. Circuit (b) also has a large cumulative error at the terrain peak. For a circuit such as Circuit (a) that crosses a bell-shaped mountain, the cumulative error is largest near the terrain peak. After the terrain peak, the cumulative error starts to decrease, and finally approaches zero when meeting the starting benchmark of the circuit. Thus the cumulative error will be nearly symmetric with respect to the peak of a bell-shaped mountain. This can be explained by Eq. (16): if H_B is greater/smaller than H_A, then the error is positive/negative, respectively. For a bell-shaped mountain, for every positive error there is a corresponding negative error, thus the cumulative error will approach zero when accumulated over the entire circuit. Figure 9 shows a strong degree of symmetry in the cumulative error, despite some small perturbations that are due to high-frequency elevation and density variations. Because of such cancellation of error, a small cumulative error along a closed circuit, for example as implied by closure statistics, does not imply small errors in OHs at the intermediate benchmarks; see more about cumulative error in the discussion of misclosure below.

4.3 Terrain correction and mean gravity in the modified Mader method

In the modified Mader method, the TC computation was split into an inner zone effect and an outer-zone effect as proposed by Forsberg (1984). The optimal radii of the inner and outer zones were found to be 30 and 100 km, respectively, based on tests of accuracy and computation efficiency. The $3'' \times 3''$ elevation grid and the $30'' \times 30''$ elevation grid were used for the inner- and outer-zone computations, respectively. Figure 10 shows a comparison of TCs along the leveling lines computed by Gaussian quadrature and FFT. The program 'tcfour' (Forsberg 1984), based on an approximated formula of the TC, was used to compute the TC by FFT. Table 3 shows statistics of TCs from Gaussian quadrature and their differences with TCs from FFT. In a rugged terrain such as that in Taiwan, these two algorithms yield different results, especially in the Central Range. Even at low elevations, differences can be significant provided that the surrounding terrain is complex. For example, one leveling line is situated along the coastal highway in northeastern Taiwan (Fig. 3), where the elevations are low. On the western flank of this highway rise mountains of over 2 km elevation, which create a large terrain effect. As seen in Fig. 10, Gaussian quadrature picks up this drastic change of terrain better than the FFT does. In general, compared to the FFT, Gaussian quadrature produces a TC that has a larger magnitude and a higher spatial resolution. This is because Gaussian quadrature makes no approximation of the given TC formula [Eq. (29)] and takes into account the maximum possible detail that the given elevation grid can provide. Note that an FFT method based on the rigorous formula of TC can also achieve high precision (see Tsoulis 2001).

In theory, of the five methods under study, the modified Mader method should deliver the most accurate OC (Heiskanen and Moritz 1967, p. 165). As shown in Figs. 6 and 7, the modified Mader method (Method 5) creates OCs that are substantially different from OCs

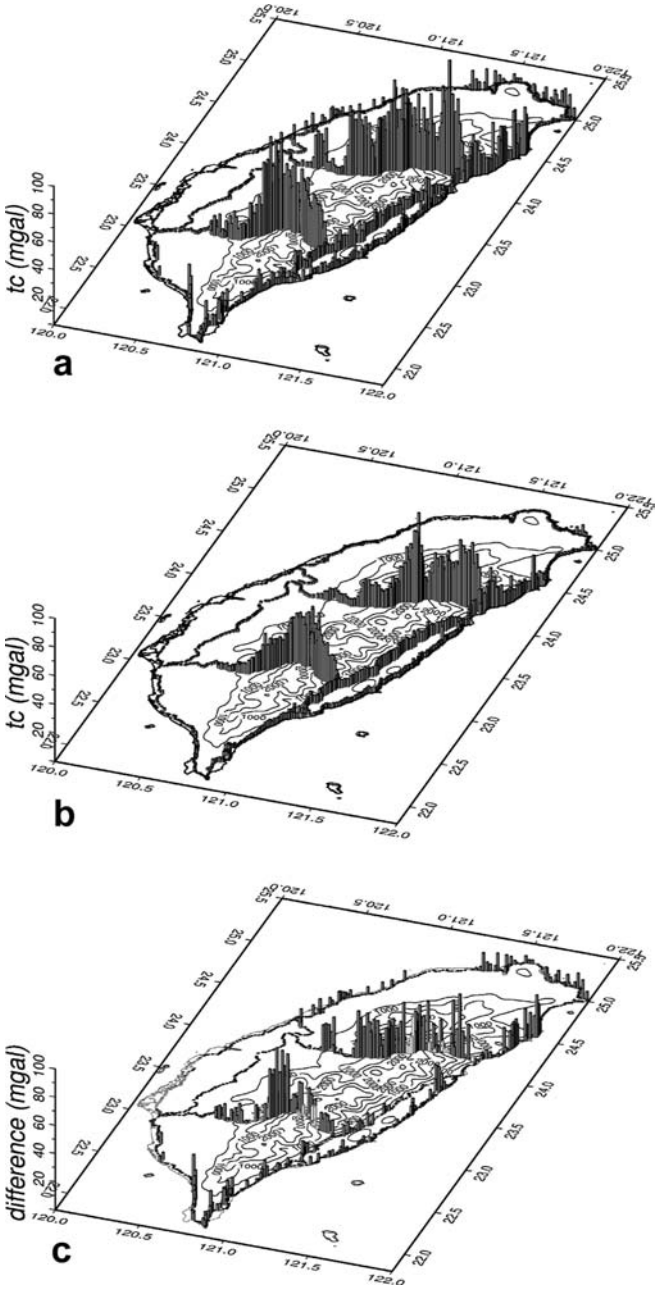

Fig. 10. Terrain corrections (TCs) from **a** Gaussian quadrature, **b** FFT, and **c** their difference

Table 3. Statistics of terrain correction (in mGal) from Gaussian quadrature (TC) and FFT at first-order benchmarks

	Maximum	Minimum	Mean	Standard deviation
TC	82.57	0.25	9.83	13.43
FFT	61.86	0.22	6.39	9.21
Difference	48.54	−26.02	3.56	7.22

created by Methods 1 and 4. The difference is obviously caused by the difference in mean gravity and the role of the TC. Figure 11 shows the difference between mean gravity values from Methods 5 and 4. The maximum,

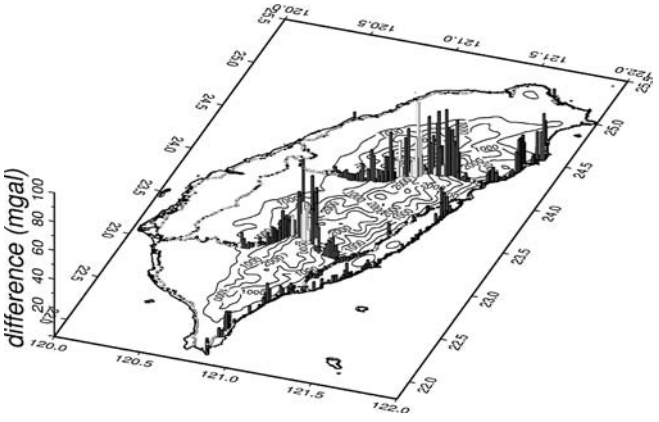

Fig. 11. Difference in mean gravity between the modified Mader method and the Helmert method with variable density and gravity anomaly gradient

maximum, mean, and standard deviation of the differences between G5 and G4 are 47.42, −51.40, 0.09, and 7.35 mGal, respectively. Large differences in mean gravity occur at high elevations and along the coastal highway in northeastern Taiwan. The pattern of differences in mean gravity is very similar to the pattern of differences in the OC (cf. Figs. 7c and 11). These differences in mean gravity are caused by many factors. First, in Method 4, the reduction of mean gravity is based on the simple Bouguer plate with the assumption that free-air gradient is valid irrespective of the existence of the mass above the geoid. In Method 5, the TC is applied and the mass above the geoid is removed while making the free-air reduction. Both Methods 4 and 5 take into account gravity anomaly gradients, but the gradients used in these two methods are different: Method 4 uses the free-air gravity anomaly gradient while Method 5 uses the Bouguer gravity anomaly gradient. As seen in Fig. 8, the free-air gravity anomaly gradients are large at high elevations, where the Bouguer gravity anomaly gradients (not shown in this paper) are also large but with different signs. Large differences in gravity anomaly gradient will cause large differences in mean gravity. In fact, in Step 2 of the modified Mader method, the free-air gravity anomaly gradient was tried instead of the suggested Bouguer gravity anomaly gradient, but the resulting mean gravity yielded even larger differences with the mean gravity from Method 4.

4.4 Misclosures of leveling circuits and results of height difference adjustments

As the OCs from the three different methods are significantly different at high elevations and at locations with complex terrains (e.g. coastal highway in northeastern Taiwan), a question arises as to which OC is the most accurate in reality, or which OC should be used for practical work in correcting geometric height differences. One way to answer this question is to compute misclosures at closed leveling circuits. In theory the sum of orthometric height differences over a closed circuit

Table 4. Misclosures (in mm) of orthometric height differences over four closed leveling circuits (Fig. 3) using different orthometric corrections

Orthometric correction	(a)	(b)	(c)	(d)
Uncorrected	117.78	−65.95	−25.35	−19.98
Helmert	21.56	−13.42	−17.49	−24.14
Helmert with variable density and anomaly gradient	19.30	−14.52	−17.96	−24.04
Modified Mader	21.31	−13.30	−17.51	−24.16

will be zero. That is, the line integral along a closed circuit satisfies

$$\oint \mathrm{d}H = 0 \tag{32}$$

where $\mathrm{d}H$ is the differential orthometric height. Table 4 shows the misclosures of orthometric height differences at the four leveling circuits shown in Fig. 3 for different cases. The case with the uncorrected height difference (i.e. geometric height difference) has the largest misclosure in most circuits. In particular, the misclosure in Circuit (a) is 117.8 mm, which is reduced to about 20 mm by any of the three OCs. Circuit (b) also receives a large reduction of misclosure by adding the OC. Curiously, the misclosure in Circuit (d) increases slightly after applying the OC. The increase may be caused by errors in OC and/or leveling. In fact, this increase is approximately equal to the average standard deviation of the estimated heights at benchmarks from LS adjustment (see below). Since the misclosures from different OCs differ only marginally, it is not possible to determine which OC is the best based on misclosures alone. However, the cumulative error in the OC will be part of the misclosure and it will remain unknown in the case of a bell-shaped terrain (see Sec. 4.2). Therefore, again, a small misclosure at a closed circuit does not necessarily mean small errors in orthometric height at individual benchmarks.

LS adjustments were also made for the uncorrected and corrected height differences at the first-order benchmarks. The stochastic model used was the standard Gausse–Markoff model (Koch 1987). The weight for each height difference was taken as the inverse distance between two benchmarks. In all adjustments, the minimum constraint solution was used by fixing the elevation at Benchmark K999 (see Fig. 3). Table 5 shows the statistics of standard deviations of adjusted OHs and the a posteriori standard errors of unit weight ($\hat{\sigma}_0$), which are descriptors of the stochastic model and data quality for the adjustments. In the case of using the same stochastic model, the smaller the a posteriori standard error of unit weight, the better the data quality. From Table 5, applying OCs indeed improves the adjustment result significantly (see the uncorrected case and the case with any of the three methods). The three OCs yield almost identical results. This implies that it is still not possible to determine which OC is the best based on the adjustment results alone. These almost identical results are attributed to the fact that large differences among the three OCs exist only at a small portion of the leveling lines (i.e. those at high elevations), and introduce little change in the standard error of height and the a posteriori standard error.

Table 5. Statistics of results of leveling adjustment using different orthometric corrections

Orthometric correction	$\hat{\sigma}_0$ (mm/$\sqrt{\text{km}}$)	Max standard error (mm)	Mean standard error (mm)
Uncorrected	2.53	25	20
Helmert	0.87	9	7
Helmert with variable density and anomaly gradient	0.88	9	7
Modified Mader	0.87	9	7

5 Conclusions

In this paper, a new formula for OC computation was presented. The OC computation requires mean gravity data along the plumb line. Five methods of mean gravity computation were tested using gravity, leveling, elevation, and density data. In one case, the Mader method is modified to take into account rock density variations and gravity anomaly gradients. The effects of variable density and gravity anomaly gradient in the Helmert method are found to be significant in computing the OC. An approach based on Gaussian quadrature is used to compute terrain effects. The five methods all yield small OCs at low elevations (except in the case where there are high mountains nearby) and large OCs (>10 cm) at high (>2 km) elevations. Furthermore, these methods produce results that are almost the same at low elevations, but significantly different (>15 cm) at high elevations. Applying the OC reduces the misclosures of height differences over closed leveling circuits and improves the overall accuracy of a leveling network. The modified Mader method is recommended for computing the OC provided that an elevation grid and free-air anomaly grids are available.

Acknowledgments. This study is supported by the Ministry of the Interior (MOI), Taiwan, under the project 'Measuring gravity on first-order benchmarks'. The authors are grateful to F.S. Ning and his colleagues at BSB (Base Survey Battalion) for their precision work in collecting gravity data, and to R. Forsberg for the terrain correction program. They also thank the Institute of Agricultural and Forestry Aerial Survey for elevation data and MOI for leveling data. Dr. Will Featherstone and three anonymous reviewers are thanked for their constructive comments.

References

Allister NA, Featherstone WE (2001) Estimation of Helmert orthometric heights using digital barcode leveling, observed gravity and topographic mass-density data over part of Darling Scarp, Western Australia. Geomat Res Aust 75:25–52

Chiou YH (1997) The generation and application of the digital terrain density model of Taiwan Area. Masters thesis, Depart-

ment of Civil Engineering, National Chiao Tung University, Hsinchu
Dennis ML, Featherstone WE (2003) Evaluation of orthometric and related height systems using a simulated mountain gravity field. Proc GG2002 Conference, Thessaloniki, Greece In: Tziavos (ed.), Ziti Editions, pp. 389–394
Forsberg R (1984) A study of terrain reductions, density anomalies and geophysical inversion methods in gravity field modeling. Rep 355, Department of Geodetic Science and Surveying, The Ohio State University, Columbus
Gerald CF, Wheatley PO (1994) Applied numerical analysis, 5th edn. Addison-Wesley, New York
Heiskanen WA, Moritz H (1967) Physical geodesy. WH Freeman, San Francisco
Hsu SK, Liu CS, Shyu CT, Liu SY, Sibuet JC, Lallemand S, Wang CS, Reed D (1998) New gravity and magnetic anomaly maps in the Taiwan–Luzon region and their preliminary interpretation. Terr Atm Ocean 9:509–532
Hwang C, Wang CG, Lee LH (2002) Adjustment of relative gravity measurements using weighted and datum-free constraints. Comput Geosci 28:1005–1015
Hwang C (1997) Analysis of some systematic errors affecting altimeter-derived sea surface gradient with application to geoid determination over Taiwan. J Geod 71:113–130
Kao S, Hsu R, Ning F (2000) Results of field test for computing orthometric correction based on measured gravity. Geomat Res Aust 72:43–60
Koch KR (1987) Parameter estimation hypothesis testing in linear models. Springer, Berlin Heidelberg New York
Mader K (1954) The orthometric weight correction of precision leveling in high terrain [in German]. Austrian Magazine for Surveying, Sp Edn 15, Vienna
Moffit FH, Bossler JD (1998) Surveying, 10th edn. Addison-Wesley, New York
Moritz H (1968) On the use of terrain correction in solving Molodensky's problem. Rep 108, Department Geodetic Science and Surveying, The Ohio State University, Columbus
Moritz H (1980) Advanced physical geodesy. Herbert Wichmann, Karlsruhe
Press WH, Flannery BP, Teukolsky SA, Vetterling WT (1989) Numerical recipes. Cambridge University Press, New York
Rapp RH, Balasubramania N (1992) A conceptual formulation of a world height system. Rep 421, Department of Geodetic Science and Surveying, The Ohio State University, Columbus
Sansò F, Rummel R (eds) (1997) Geodetic boundary value problems in view of the one centimeter geoid. Lecture Notes in Earth Sciences, vol 65. Spinger, Berlin Heidelberg New York
Schwarz KP, Sideris M, Forsberg R (1990) The use of FFT techniques in physical geodesy. Geophys J Int 100:485–514
Strang van Hees GL (1992) Practical formula for the computation of orthometric, dynamic and normal heights. Z Vermess 11:727–734
Torge W (1989) Gravimetry. Walter de Gruyter, Berlin
Tsoulis D (2001) Terrain correction computations for a densely sampled DTM in the Bavarian Alps. J Geod 75:291–307
Vaníček P, Janák J, Huang J (2000) Mean vertical gradient of gravity. In: Sideris MG (ed) Gravity geoid and geodynamics 2000. Springer, Berlin Heidelberg New York, pp. 259–262
Wessel P, Smith WHF (1995) New version of the Generic Mapping Tool released. EOS Trans Am Geophys Union 76:329
Yen HY, Yeh HY, Lin CH, Yu GK, Tsai YB (1990) Free-air gravity map of Taiwan and its applications. Terr Atm Ocean 1:143–156